Tellus (2008), 60A, 305–320
Printed in Singapore. All rights reserved

TELLUS

A simple and efficient locally mass conserving semi-Lagrangian transport scheme

By EIGIL KAAS*, *Niels Bohr Institute, University of Copenhagen, Denmark*

(Manuscript received 7 August 2007; in final form 5 November 2007)

ABSTRACT

A new simple and accurate locally mass conserving semi-Lagrangian (LMCSL) scheme has been constructed. Mass conservation is obtained by introducing modified interpolation weights at the upstream departure points. Thereby the total mass given off by a given Eulerian grid point to all the surrounding semi-Lagrangian (SL) departure points is equal to the cell area represented by that grid point. The new scheme is equivalent to the cell-integrated semi-Lagrangian (CISL) transport schemes in the sense that divergence—via the weights—is determined by the trajectories and not by centred differences as in traditional SL-schemes.

The LMCSL scheme has been combined with the semi-implicit scheme in a shallow water model. Thereby a numerically stable and inherently mass conserving scheme permitting long time steps has been set up. Tests in plane horizontal geometry including topography give solutions very similar to those obtained with the traditional semi-implicit SL scheme. The well known mountain wave resonance problem appears to be reduced.

The increase in numerical cost of the new scheme relative to traditional SL models is small, particularly when there are several passive tracers, since the same weights are used for all tracers.

1. Introduction

New generations of atmospheric circulation models for use in numerical weather prediction (NWP) and climate research include the individual densities of an increasing number of particles and chemical tracers, as prognostic variables. These variables are introduced to be able, in a consistent way, to forecast and simulate the evolution of air pollution and air chemistry, to simulate the direct radiative effects of the tracer constituents, and to simulate the indirect effects of some particles (CCN's) on cloud microphysics. By consistent is here meant that the evolution of the chemical constituents are based on the same numerical techniques and with the same resolution in both time and space as the physical model. Consistency is of importance for obtaining accurate simulations of one and two-way interactions between the physical atmosphere (including clouds and precipitation) and atmospheric chemistry. The issue of model internal consistency has been discussed in detail in Jöckel et al. (2001).

Rasch and Williamson (1990) have defined seven desirable properties for transport schemes, that is, numerical schemes designed for solving the continuity equation: accuracy, stability, computational efficiency, transportivity, locality, conservation and shape-preservation.

*Correspondence.
e-mail: kaas@gfy.ku.dk
DOI: 10.1111/j.1600-0870.2007.00293.x

Obviously, accuracy and computational efficiency are interrelated since in real applications, where the computer resource is given, it often pays off to enhance the spatial resolution, that is, the number of grid points, at the expense of the formal numerical accuracy. Also stability can be related to computational efficiency: for example, semi-implicit (SI) integration schemes (Robert et al., 1972) are known for their high numerical stability even for long time steps. However, SI-schemes involve the solution of an elliptic equation, and this is generally less efficient on massive parallel computers due to considerable data-interchange between the computational nodes.

The transportivity and locality properties of a scheme refer to its ability to transport information along the characteristics, and that only adjacent grid values affect the forecast at a given point. Generally Lagrangian and semi-Lagrangian (SL) schemes tend to be more 'transportive' than Eulerian schemes, and by definition traditional spectral models are non-local.

Formal conservation of mass is important for atmospheric constituents with a relatively long residence time in the atmosphere. The notion 'local mass conservation' refers to the inherent ability of a scheme to conserve mass along characteristics, that is, simultaneous fulfilment of the conservation and transportivity/locality properties.

The shape preservation property states that no artificial local maxima or minima should evolve due to the numerics. This property encompass the positive definiteness property which is the ability of a scheme to maintain only positive densities in an

initially positive density field. Natively most numerical schemes—except for strongly damping schemes—are non shape preserving. Shape preservation can be obtained, though, by introducing certain filters such as the flux based filter (Zalezak, 1979), or for SL models a filter as in Zerroukat et al. (2005).

Desirable properties in addition to those described in Rasch and Williamson (1990) have emerged in the literature. Two of the most important are consistency (Jöckel et al., 2001), mentioned above, and preservation of constancy in non-divergent flow (e.g. Staniforth and Coté, 1991).

The consistency property concerns the coupling between the continuity equation for air as a whole and for individual tracer constituents. Traditionally the mixing ratio is used as prognostic variable for chemical and water constituents. The local density is then the product of the mixing ratio and the density of air. However, unless on uses consistent numerical schemes, the same time step and the same grid spacing to obtain the mixing ratio and the density of air, it is not trivial to ensure formal local mass conservation of a tracer. Therefore, consistency between numerical schemes is essential. In general consistency cannot be achieved for off line chemical models unless special care is taken. Even for on-line models consistency is hard to obtain. For example it is not formally achieved in semi-implicit models because the semi-implicit correction introduces a (non-local) modification of the native numerical scheme used for density of air. A needed corresponding modification is generally not considered for the tracers.

The constancy preservation in non-divergent flows is trivially obtained in traditional SL schemes since the divergence of the velocity field does not appear in the prognostic equation for mixing ratio. However, for finite-volume methods, where the divergence appears explicitly since tracer density and not mixing ratio is the prognostic variable, it is not automatic that a constant field is preserved for a non-divergent velocity field.

The perfect scheme for solving the continuity equation would have all the desirable properties listed above. However, so far, in practice, no method is advantageous under all conditions.

Semi-implicit SL schemes (SISL) initially introduced by Robert (1981, 1982) have proven very accurate and efficient for solving the atmospheric equations of motion in both hydrostatic and non-hydrostatic models. Several of the present day operational forecast systems such the IFS operated at the European Centre for Medium-Range Weather Forecasts (ECMWF) and the Nordic High Resolution Limited Area Model (HIRLAM) are based on SISL-schemes. Although being highly cost-effective SISL models suffer from a number of serious disadvantages making them less suited as building bricks for the future generations of NWP and Earth System models. The most important problems are that SISL models are not conservative and that they—in their traditional form—have only been made shape conserving using filters that tend to smooth strongly varying densities.

A number of recent and less recent conservative SL—or 'SL-like'—methods (e.g. Laprise and Plante, 1995; Leslie and Purser, 1995; Rančić, 1995; Leonard et al., 1996; Lin and Rood, 1996; Nair and Machenhauer, 2002; Nair et al., 2002; Xiao et al., 2002; Zerroukat et al., 2002; Lin, 2004; Zerroukat et al., 2006; Lauritzen et al., 2006; Zerroukat et al., 2007; Cotter et al., 2007; Reich, 2007) have been suggested and tested in atmospheric models. These schemes not only benefit from the accuracy and numerical stability of the original interpolating grid point SL schemes but also have the conservation property advantages of their Eulerian counterparts. Thus, these schemes already fulfil a number of the desired properties listed above.

One of the issues left is the shape-preservation. Zerroukat et al. (2006) and Zerroukat et al. (2007) have designed an efficient filter which, on top of its basic monotonicity properties, also enhances the numerical accuracy for a series of numerical problems.

Although some of the schemes and methods listed above already have been implemented as part of the dynamical cores in general circulation models there still remain issues for some of the schemes such as

(i) optimal generalization to three dimensions,
(ii) the mass-wind inconsistency problem,
(iii) the preservation of constancy in non-divergent flow, and
(iv) introduction of techniques controlling numerical instability related to gravity and sound waves.
(v) Furthermore, there is still room for improvements of the basic numerical performance of the schemes.

The final goal of the present ongoing work is to formulate and test a new transport scheme which fulfils most, if not all, the properties discussed above to a satisfactory extent. As such the new scheme may—in its final form—be considered as an alternative to the SLICE (Zerroukat et al., 2007), the CISL (Lauritzen et al., 2006) and the flux based schemes of Lin and Rood (1996) and Xiao et al. (2002). The first step, presented here, towards formulating a new transport scheme has been to formulate and test a new simple locally mass conserving semi Lagrangian (LMCSL) scheme and to combine this scheme with the semi-implicit scheme.

The second ingredient in the new transport scheme—to be presented and tested in a subsequent paper—is a new monotonic Lagrangian filter. In addition to ensuring shape conservation this filter is formulated in such a way that it also fulfils the requirement of preservation of constancy in non-divergent flows. Furthermore, the new filter enhances the numerical accuracy near sharp gradient variations.

This paper is organized as follows. The mathematical formulations behind the new scheme are explained in Section 2. In Section 3 this is followed by a few passive advection tests in two dimensions comparing the traditional SL scheme and the LMCSL scheme, both based on bicubic interpolations. The combination of the semi-implicit scheme with the LMCSL scheme is described in Section 4 while Section 5 shows results from a few test simulations where the new semi-implicit LMCSL (SI-LMCSL) scheme is compared with a traditional SISL

scheme. A discussion of generalizations, numerical costs and remaining problems can be found in Section 6, and a short summary of the results obtained is provided in Section 7.

2. Locally mass conserving semi-Lagrangian formulation

In SL models the Lagrangian form of the continuity equation is used to describe the temporal evolution of density per unit volume ψ

$$\frac{\mathrm{d}\psi}{\mathrm{d}t} = -\psi \nabla \cdot \mathbf{v}, \tag{1}$$

where $\mathbf{v}$ is the velocity field in one, two or three dimensions depending on the problem. Note, though, that in atmospheric models the vertical problem is often separated and treated in a different way as mentioned in Section 6.2.

The first element in SL schemes is an iterative procedure for determining all trajectory departure points at a given time step n ending up in the Eulerian grid points at time step $n+1$. This issue will be discussed in more detail in Section 4.1.

Once the Lagrangian departure points are found the traditional explicit SL approach for integrating (1) forward in time for a given Eulerian grid point k normally takes a form such as

$$\psi_k^{n+1}{}_{\mathrm{SL-exp}} = \psi_{*_k}^n - \Delta t \, (\psi \nabla \cdot \mathbf{v})_{*_k/2}^{n+1/2}, \tag{2}$$

where n is the time step number, Δt the length of the time step, $(\cdot)_{*_k}^n$ a spatially interpolated value at the trajectory departure point, and $(\cdot)_{*_k/2}^{n+1/2}$, formally valid at the trajectory mid-point, is an estimate based on interpolations in space and extrapolations in time from the previous time steps.

Different methods have been used to estimate the last term on the right-hand side in eq. (2). In this paper the following approach is used to obtain a traditional explicit SL-forecast:

$$\begin{aligned}\psi_k^{n+1}{}_{\mathrm{SL-exp}} = {} & \{\psi - 0.5\Delta t(\psi \nabla \cdot \mathbf{v})\}_{*_k}^n \\ & - 0.5\Delta t(\psi \widetilde{\nabla \cdot \mathbf{v}})_k^{n+1},\end{aligned} \tag{3}$$

where $\widetilde{(\cdot)}$ indicates a value that has been extrapolated linearly in time from time steps $n-1$ and n to $n+1$. This corresponds to the methodology in Temperton and Staniforth (1987). Using the notation $\widetilde{(\cdot)}^{n+1} = 2(\cdot)^n - (\cdot)^{n-1}$ to indicate such extrapolation will be applied throughout the paper.

The traditional SL scheme (3) can also be written as

SL scheme

$$\begin{aligned}\psi_k^{n+1}{}_{\mathrm{SL-exp}} = {} & \sum_{l=1}^{K} w_{k,l}\left[\psi_l^n - 0.5\Delta t(\psi \nabla \cdot \mathbf{v})_l^n\right] \\ & - 0.5\Delta t \left(\psi \widetilde{\nabla \cdot \mathbf{v}}\right)_k^{n+1},\end{aligned} \tag{4}$$

where k is a multidimensional Eulerian grid point index, K is the total number of (multidimensional) Eulerian grid points, and $w_{k,l}$ are the weights given to the upstream Eulerian grid points l, representing the polynomial upstream interpolations to the Lagrangian departure point $(\cdot)_{*_k}$ of the trajectory ending up in the Eulerian grid point k. These weights will be denoted 'SL-weights' in the following and they will only be different from zero in the grid points l surrounding the departure point.

The SL-weights define the re-mappings from the departure points to the Eulerian points and they depend on the location of the trajectory departure point and on the order of the interpolation scheme used. Once these weights are determined for all departure points at a given time step they can be used to forecast the densities for all tracers as well the density of air. Note that for any traditional SL scheme in any spatial dimension we have

$$\sum_{l=1}^{K} w_{k,l} = 1. \tag{5}$$

As mentioned in the introduction traditional SL schemes based on upstream interpolations are not mass conserving. An other way to express this is that the total mass given off by a given Eulerian grid point at time level n to all the surrounding departure points, including the mass related to the divergence term in (2), is different from the mass represented by that particular grid point. Inspired by the philosophy behind the so-called cell-integrated semi-Lagrangian (CISL) schemes (e.g. Machenhauer and Olk, 1997) it is, however, possible to reformulate the explicit discrete form of the full continuity equation (including the divergence term) in a very simple way by introducing a localized so-called partition of unity. This means that we define modified upstream weights $\hat{w}_{k,l}$ to obtain the following mass conserving quasi local scheme:

LMCSL scheme

$$\begin{aligned}\overline{\psi}_k^{n+1}{}_{\mathrm{LM-exp}} = {} & \left\{\overline{\psi}\right\}_{**_k}^n \\ \equiv {} & \sum_{l=1}^{K} \hat{w}_{k,l}, \overline{\psi}_l^n\end{aligned} \tag{6}$$

where

$$\hat{w}_{k,l} = \frac{A_l}{A_k} \frac{w_{k,l}}{\sum_{m=1}^{K} w_{m,l}} \tag{7}$$

with $w_{k,l}$ identical to the grid point SL-weights and A_k being the volume represented by the kth Eulerian grid point, that is, the size of the Eulerian grid cell. The over lines in (6) indicate spatial averages over the Eulerian grid cells since, contrary to the SL scheme, the LMCSL scheme simulates the evolution of the grid cell averages and not the grid point values. We will use the name 'LMCSL' for the new locally mass conserving semi Lagrangian integration scheme in (6). The formulation in (6) is general in the sense that any type or order of interpolation can be used as long as it is possible to identify SL-weights to each Eulerian grid point/cell.

Under the assumption that we have a closed/periodic domain it can easily be seen that the total mass of the forecast is equal to the total mass of the original field:

$$\begin{aligned}\sum_{k=1}^{K} A_k \overline{\psi}_k^{n+1}{}_{\mathrm{LM-exp}} &= \sum_{k=1}^{K}\sum_{l=1}^{K} A_k \hat{w}_{k,l} \overline{\psi}_l^n \\ &= \sum_{k=1}^{K}\sum_{l=1}^{K} \frac{A_l w_{k,l}}{\sum_{m=1}^{K} w_{m,l}} \overline{\psi}_l^n \\ &= \sum_{l=1}^{K} A_l \frac{\sum_{k=1}^{K} w_{k,l}}{\sum_{m=1}^{K} w_{m,l}} \overline{\psi}_l^n = \sum_{l=1}^{K} A_l \overline{\psi}_l^n \end{aligned} \quad (8)$$

and so we have formal mass conservation. In other words: the new modified SL-weights ensure that the total mass given off by any Eulerian grid point to all the surrounding departure points is exactly equal to the mass represented by that grid point.

The LMCSL scheme in its general form (6) is not strictly locally mass conserving because the polynomial weights remap mass from a number of Eulerian grid cells in a certain domain surrounding the departure point. The degree of locality depends on the desired accuracy of the polynomials: the higher accuracy the less locality. This is fully equivalent to the situation in any finite volume scheme (e.g. Lin and Rood, 1996; Nair and Machenhauer, 2002; Zerroukat et al., 2007), because in such schemes it is necessary to make analytical subgrid-cell reconstructions for each grid cell. The reconstructions are used to enable the needed upstream spatial integrations of mass. They are based on information from grid cell averages in a domain surrounding the target cell. It is the reconstructions which introduces some non-locality. The degree of non-locality in LMCSL is equivalent to the degree of non-locality in any finite volume scheme with equivalent numerical accuracy in the subgrid-cell reconstructions. Since finite volume schemes are generally referred to as locally mass conserving, it has been chosen to also include the new scheme in the class of locally mass conserving schemes. As for finite volume schemes this notion only makes sense if the order of the polynomial representations is fairly small, that is, not much higher order than the (bi)cubic which is used in the present application.

The LMCSL scheme is quite similar to the so-called 'Remapped particle-mesh semi-Lagrangian advection scheme' by Cotter et al. (2007) and even more so to the modified version of this scheme by Reich (2007). The original scheme by Cotter et al. (2007) involves solution of an implicit set of linear equations which is needed to obtain modified weights analogue to those in (7) but for a downstream trajectory SL scheme. In the modified scheme by Reich (2007) an explicit modification of the downstream weights are introduced. It is even demonstrated that the methodology may be modified to handle the upstream SL approach as used in this paper, however, only for the non-divergent passive advection equations.

The LMCSL scheme is somewhat similar to the CISL scheme:

CISL scheme

$$\overline{\psi}_k^{n+1}{}_{\mathrm{CI-exp}} = \left(\frac{\delta V}{\Delta V}\right)_k \overline{\psi}_{*_k}^n, \quad (9)$$

where the overlining (as for LMCSL) indicates a spatial grid cell average, and δV and δV are the SL departure volume and the Eulerian arrival grid cell volume, respectively. The SL departure volume average ($\overline{\psi}_{*_k}^n$) is obtained via spatial integration requiring considerable computer resources.

In CISL schemes (see e.g. Lauritzen et al., 2006), divergence is defined from the divergence of the SL trajectories. Divergence of trajectories results in Lagrangian departure volumes that are generally different from the arrival Eulerian grid cell volumes. This leads to the CISL definition of divergence:

CISL divergence

$$\mathcal{D}_k^{n+1/2}{}_{\mathrm{CI}} = \frac{1}{\Delta t}\left(1 - \delta V/\Delta V\right)_k, \quad (10)$$

where superscript $n + 1/2$ indicates that the trajectories determining δV are defined from the velocity field both at time level n and at (the extrapolated) time level $n + 1$.

In the LMCSL scheme divergence is defined in a way analogue to that in CISL:

LMCSL divergence

$$\mathcal{D}_k^{n+1/2}{}_{\mathrm{LM}} = \frac{1}{\Delta t}\left(1 - \sum_{l=1}^{K} \hat{w}_{k,l}\right). \quad (11)$$

To understand (11) intuitively we can consider a situation with no or little divergence. In this case the spatial density of upstream trajectory departure points is equal or close to the density of the Eulerian grid points. This means that $\hat{w}_{k,l}$ tends to be close to or equal to 1, whereby $\mathcal{D}_k^{n+1/2}{}_{\mathrm{LM}}$ is close to zero, and the forecast is close to the SL-scheme (4) with the divergence terms set to zero. In a situation with (positive) divergence in a given region the trajectories will diverge, that is, departure points will be spatially more dense than in the case of no divergence. This means that $\hat{w}_{k,l}$ will be less than one whereby the forecasted density—as expected—is smaller than in the non-divergent situation.

With reference to the description of the semi-implicit version of the LMCSL scheme in Section 4 it is important to note that the LMCSL way of treating divergence is fundamentally different from the centred difference treatment used in most Eulerian or SL grid point models.

In practice it is straightforward to calculate the modified SL-weights. As compared to the traditional SL approach it requires an additional loop over all grid points where the SL-weights are calculated. During this loop the weights need to be summed in a separate array to obtain the denominator in (7). Once the modified weights are defined they can be used to update the time integration for all prognostic density variables at a given time step.

3. Passive advection tests in plane geometry

Non-divergent passive advection tests based on bicubic upstream interpolations have been performed in two dimensions in plane geometry. The test cases have been mainly chosen to enable comparison with other similar transport published schemes (e.g. Hólm, 1995; Nair et al., 1999; Zerroukat et al., 2002; Cotter et al., 2007; Zerroukat et al., 2007). They include solid body rotation of a slotted cylinder, a cosine hill and a cone at different spatial resolutions. Furthermore, the idealized cyclogenesis problem originally proposed by Doswell (1994) has been tested.

3.1. Solid body rotation tests

In the solid body rotation experiments the density field rotates with constant angular velocity ω about a point (x_c, y_c).

For the slotted cylinder the analytical—that is, the true—solution is

$$\psi^t(x, y, t) = \begin{cases} \psi_0 & \text{for } |\xi| \geq s_w/2 \text{ and } r \leq \sigma, \\ \psi_0 & \text{for } \zeta \geq s_l - \sigma \text{ and } r \leq \sigma, \\ 0 & \text{otherwise,} \end{cases} \tag{12}$$

with ψ_0 a constant, σ the cylinder radius, and s_l, s_w the length and width of the slot, respectively. The relative position coordinates, ξ and ζ are defined with respect to the rotating centre of the cylinder

$$\begin{aligned} \xi &= x - x_c + \gamma \cos(\omega t), \\ \zeta &= y - y_c + \gamma \sin(\omega t), \end{aligned} \tag{13}$$

where γ is the distance from the centre of the flow (x_c, y_c) to the centre of the cylinder $[x_c - \gamma \cos(\omega t), y_c - \gamma \sin(\omega t)]$. In (12) $r = \sqrt{\xi^2 + \zeta^2}$ is the Euclidian distance from the centre of the cylinder.

The cosine hill and cone problems are similar to the slotted-cylinder one. The analytical solution for the cosine hill problem is

$$\psi^t(x, y, t) = \begin{cases} \psi_0 \left[1 + \cos(\pi r/\sigma)\right]/2 & \text{for } r \leq \sigma, \\ 0 & \text{otherwise,} \end{cases} \tag{14}$$

and for the cone problem it is

$$\psi^t(x, y, t) = \begin{cases} \psi_0 \left[1 - r/\sigma\right] & \text{for } r \leq \sigma, \\ 0 & \text{otherwise} \end{cases} \tag{15}$$

with the same definitions for ψ_0, σ and r as for the slotted cylinder problem.

3.2. Idealized cyclogenesis problem

The setup of the idealized cyclogenesis problem in plane geometry follows that in Nair et al. (1999), Zerroukat et al. (2002) and Cotter et al. (2007). The flow is a steady circular vortex with a tangential velocity $v_T(r) = v_0 \tanh(r)/\cosh^2(r)$, where r is the radial distance from the centre of the domain and v_0 is a value chosen such that the maximum value of v_T never exceeds unity. The analytical solution is

$$\psi^t(x, y, t) = -\tanh\left[\frac{y - y_c}{\delta}\cos(\omega t) - \frac{x - x_c}{\delta}\sin(\omega t)\right]. \tag{16}$$

3.3. Experimental setup and verification

For all the problems the analytical solutions in (12), (14), (15) and (16) are used to initialize the numerical integrations at time $t = 0$. Traditionally, the 'classical' SL models are initialized with grid point values and CISL schemes with cell average values. Here we also use grid point values for the SL scheme. For the LMCSL scheme where the prognostic variable is supposed to represent the average mass in each grid cell we use Eulerian cell average values as initial prognostic variable. The cell average values of the analytical solutions to the above problems are obtained from a high-order subgrid numerical integration of the expressions in (12), (14), (15) and (16). For calculation of error measures of the numerical schemes (below) we always verify against the Eulerian cell average values of the true solution. For the LMCSL scheme this enables a direct comparison with, for example, the cell average results presented in Zerroukat et al. (2002) and Zerroukat et al. (2007). Since the traditional SL scheme is operating on grid points a cell average value has to be estimated before the statistics involving cell averages can be calculated for this scheme. This is done by integrating two-dimensional fourth-order polynomials over each grid cell. These polynomials are obtained from the forecasted grid point values. It is noted that the use of estimated SL cell averages slightly favour the scores for the LMCSL scheme over the SL scheme, because cell average is the native prognostic variable in the LMCSL scheme. The grid cell average verification for the SL scheme was introduced to accomplish a fair treatment of the SL scheme relative to the LMCSL scheme. This is because cell average verifications as used here generally score considerably better than grid point verifications, which is normally used for SL schemes.

As is customary in these type of test problems true (i.e. analytical) upstream trajectories are used. Note that in the two-dimensional test cases performed here the use of analytical trajectories does not in general imply that the denominator in (7) is equal to one. In the case of an initial non-trivial constant field value one can, therefore, expect the LMCSL scheme to produce forecast values which are different from the true initial value. This is a feature which is also typical for CISL type schemes.

For all test cases the following statistics have been calculated:

$$\text{rms} = \sqrt{\frac{1}{K}\sum_{k=1}^{K}\left(\overline{\psi}_k - \overline{\psi}_k^t\right)^2} \tag{17}$$

$$l_1 = \frac{\sum_{k=1}^{K} |\overline{\psi}_k - \overline{\psi}_k^t|}{\sum_{k=1}^{K} |\overline{\psi}_k^t|} \tag{18}$$

$$l_2 = \frac{\sqrt{\sum_{k=1}^{K} \left(\overline{\psi}_k - \overline{\psi}_k^t\right)^2}}{\sqrt{\sum_{k=1}^{K} \left(\overline{\psi}_k^t\right)^2}} \tag{19}$$

$$l_\infty = \frac{\max\left(|\overline{\psi}_k - \overline{\psi}_k^t|\right)}{\max\left(|\overline{\psi}_k^t|\right)} \tag{20}$$

$$h_{\max} = \frac{\max(\overline{\psi}) - \max(\overline{\psi}^t)}{S^t} \tag{21}$$

$$h_{\min} = \frac{\min(\overline{\psi}) - \min(\overline{\psi}^t)}{S^t}, \tag{22}$$

where

$$S^t = \max(\overline{\psi}^t) - \min(\overline{\psi}^t) \tag{23}$$

and where superscript t denotes the true value at some time and $\overline{\psi}$ an Eulerian grid cell average value.

Examples of the simulated distribution of density for each of the test cases are shown in Figs. 1–4. The spatial resolutions used in the experiments are those most frequently used as reference in the literature and listed in Tables 2, 4, 6 and 7. Only results for the LMCSL scheme are shown, since the results for the traditional SL scheme are practically indistinguishable from these at the plotting level. Some of the well-known problems with traditional SL schemes are easily seen for the bicubic interpolation scheme used here: lack of shape preservation near sharp spatial variations in gradients and some smoothing. Regarding the first of these problems this leads to artificial negative concentrations in the numerical solution and to overshoots with values higher than the analytical solution near sharp gradients in the slotted cylinder and in the cyclogenesis experiments.

Tables 1, 3 and 5 summarises the results for the solid body rotation experiments after one full rotation for different spatial resolutions. To enable comparison with other results in the literature we also in Table 2 provide results after six full rotations for the slotted cylinder problem and for two rotations for the cosine hill and the cone problems, respectively, in Tables 4 and 6. Finally, Table 7 lists the verification statistics for the cyclogenesis test at different resolutions. It is noted that all the tables will serve as references in a follow up paper where a new accurate Lagrangian monotonic filter is introduced.

The total mass in the LMCSL scheme is conserved to machine precision while in the experiments with the SL scheme the total variations in mass during the simulations are in the order of a per mile.

In summary the results with the new LMCSL scheme are very similar to those obtained with the traditional SL scheme. The differences in the tables are mainly due to the verification technique where, for the SL-scheme, the cell average values are obtained as an estimate based on the forecasted grid point values.

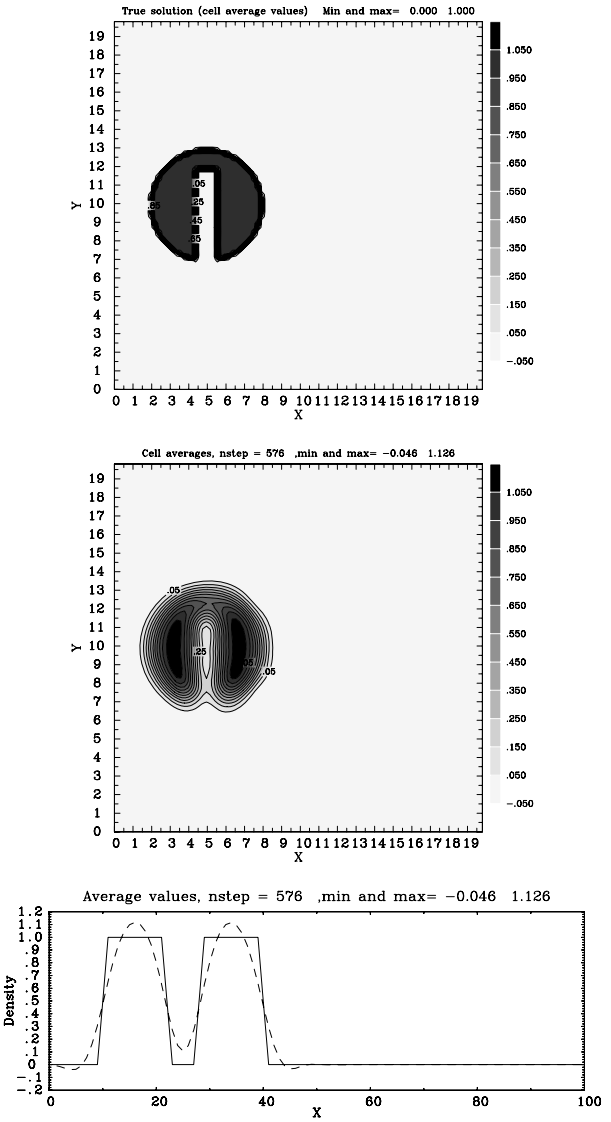

Fig. 1. Slotted cylinder solid body rotation test with the LMCSL scheme after 6 full rotations and a resolution of 101 × 101 points, that is, corresponding to the data listed in table 2. Top panel: analytical solution ($\overline{\psi}^t$). Middle panel: Numerical solution ($\overline{\psi}$) Lower panel: Cross-section in the *x*-direction through the centre y-value, with full line showing the analytical solution and the dashed line the LMCSL solution. At the top of each panel the minimum and maximum of the numerical solution is shown.

4. A semi-implicit shallow water application

It is standard procedure to use the shallow water equations as test bed for introduction of new numerical methods. The tests

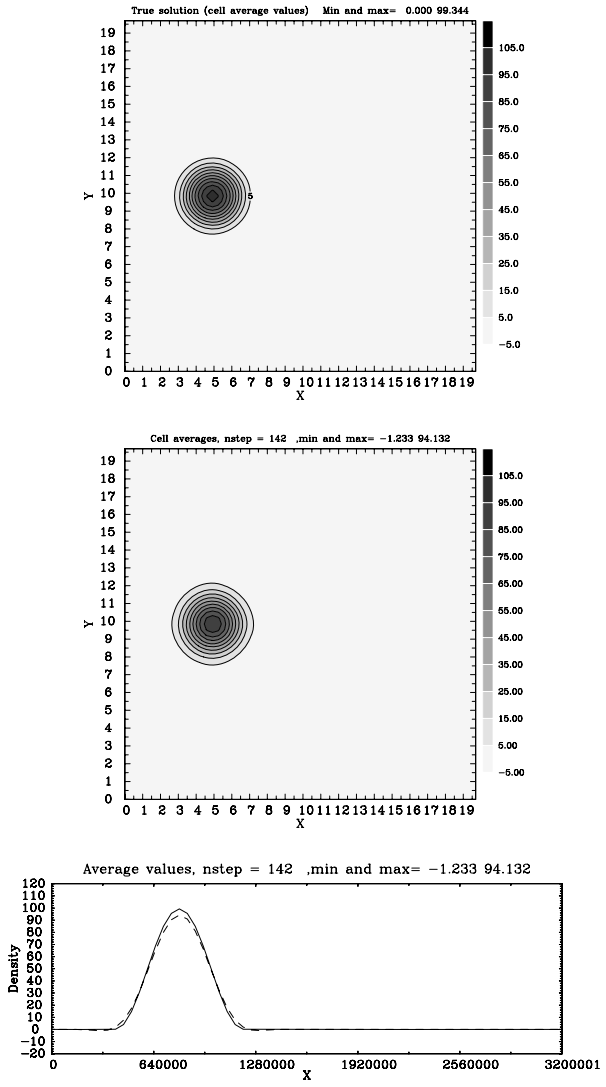

Fig. 2. As Fig. 1 but for the cosine hill problem with a resolution of 65×65 points, and after only two full rotations corresponding to the data in Table 4.

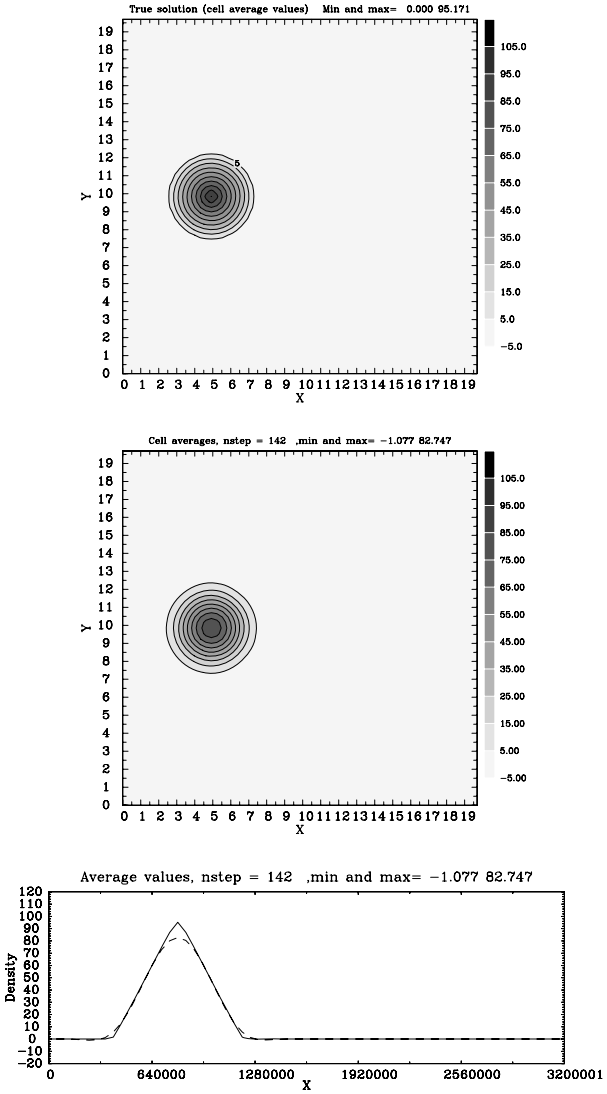

Fig. 3. As Fig. 1 but for the rotating cone problem with a resolution of 65×65 points, and after only two full rotations corresponding to data in Table 6.

presented here are performed with a relatively simple shallow water model formulated in Cartesian geometry, but with sinusoidal variation of the Coriolis parameter. The governing differential equations are

$$\begin{aligned}
\frac{\mathrm{d}u}{\mathrm{d}t} &= fv - \frac{\partial(\phi + \phi_s)}{\partial x} \\
\frac{\mathrm{d}v}{\mathrm{d}t} &= -fu - \frac{\partial(\phi + \phi_s)}{\partial y} \\
\frac{\mathrm{d}\phi}{\mathrm{d}t} &= -\phi \nabla \cdot \mathbf{v} + F \\
\frac{\mathrm{d}\psi}{\mathrm{d}t} &= -\psi \nabla \cdot \mathbf{v}, \qquad (24)
\end{aligned}$$

where u, v are the flow speed components in the x, y plane, ϕ is the geopotential thickness of the flow, ϕ_s is the stationary surface geopotential ('topography'), ψ is the horizontal density of a passive tracer and f the Coriolis parameter. F is a weak globally mass conserving Newtonian relaxation towards the initial 'zonal' average profile of ϕ.

The motivation for introducing also a passive tracer is mostly related to subsequent studies on monotonicity, positive definiteness, the mass-wind inconsistency, etc. in a fully non-linear flow. Here, however, it also serves as a basic check that a passive tracer with sharp spatial variations can be simulated reasonably well with the LMCSL scheme as compared to the SL scheme.

The setup of the model is designed to mimic a global model domain, and it has previously been used in a three time level version (Kaas et al., 1997). Here it is tested in a two time

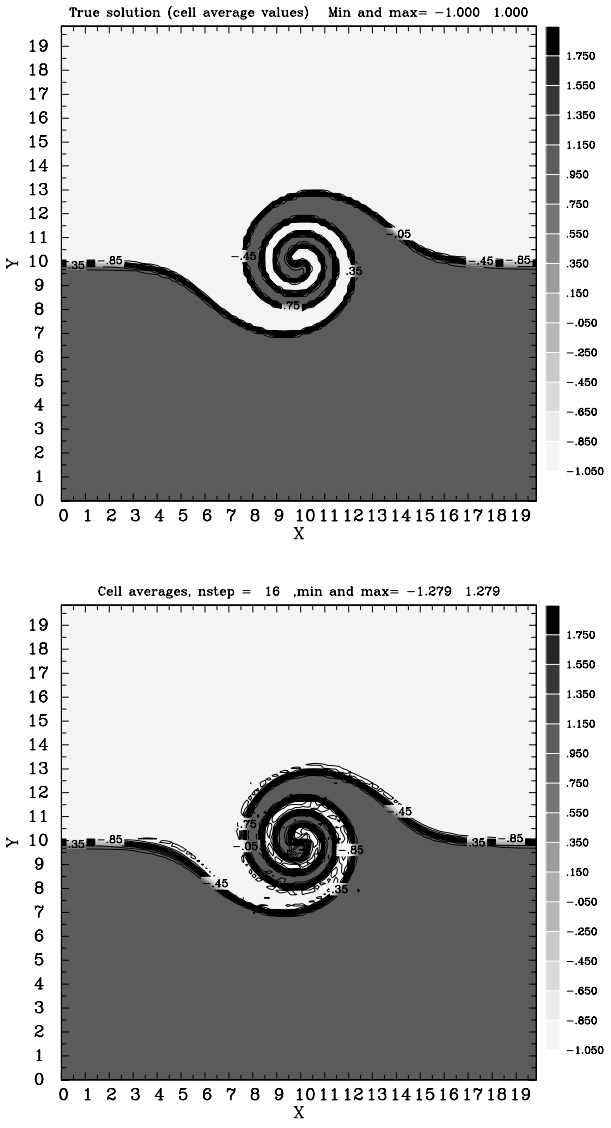

Fig. 4. As Fig. 1 (upper two panels) but for the cyclogenesis problem after 16 time steps at a resolution of 129 × 129 grid points. See Table 7 and text for details.

level setup. The integration domain covers an area of 20 000 × 20 000 km with periodic boundary conditions in both directions and with enforced symmetry around a centre line ('Equator') in the x direction for the variables u, ϕ, ϕ_s, F and ψ, and antisymmetry around the same line for the parameters v and f.

In this section, we will demonstrate that it is possible to combine the new LMCSL scheme with a semi-implicit scheme analogue to that presented in Bates et al. (1993). As in Lauritzen et al. (2006) only the solution of the mass-field equation has been modified as compared to traditional SL-models with no changes introduced in the SL-formulation of the momentum equations. The upstream trajectory algorithm used for the momentum and the mass fields is, however, slightly more advanced than in many traditional SL models.

The following Section 4.1 describes the methodology used to calculate the SL-trajectories which needs special attention because divergence is determined by these trajectories. This is followed in Section 4.2 by a description of the traditional SISL scheme on which the new SI-LMCSL scheme is based. In Section 4.3 the modifications needed for the LMCSL scheme are explained. For simplicity we will omit grid point referencing indices.

4.1. Estimation of trajectories

The first step in the SL algorithm is computation of the trajectories ending up in the Eulerian grid points at time level $n + 1$. As is common procedure the algorithm used to determine the location $\mathbf{r}_*^n$ of the trajectory departure points works iteratively. Each trajectory is split into a part involving only velocities extrapolated to time level $n + 1$ and a part involving only velocities at time level n. Following the description in Lauritzen et al. (2006) this is done by splitting the trajectory into two segments:

1. The first contribution is the trajectory from the departure point $\mathbf{r}_*^n$ to the trajectory midpoint $\mathbf{r}_{*/2}^{n+1/2}$. Approximating this half-trajectory with a Taylor series expansion about the departure point, only velocities at time-level n are used. The Mth order approximation is given by

$$\mathbf{r}_{*/2}^{n+1/2} = \mathbf{r}_*^n + \mathbf{C}_1, \tag{25}$$

where

$$\mathbf{C}_1 = \frac{\Delta t}{2}\mathbf{v}_*^n + \sum_{m=1}^{M-1} \frac{1}{(m+1)!}\left(\frac{\Delta t}{2}\right)^{m+1}\left(\frac{\mathrm{d}^m\mathbf{v}}{\mathrm{d}t^m}\right)_*^n. \tag{26}$$

The first guess departure point is the arrival point r^{n+1}. The total derivative is approximated as in McGregor (1993), that is, by discarding the Eulerian velocity change over the period from time level n to $n + 1/2$:

$$\frac{\mathrm{d}\mathbf{v}}{\mathrm{d}t} \approx \mathbf{v}\cdot\nabla\mathbf{v}. \tag{27}$$

If needed higher-order derivatives can be defined recursively as

$$\frac{\mathrm{d}^m\mathbf{v}}{\mathrm{d}t^m} = \frac{\mathrm{d}}{\mathrm{d}t}\left(\frac{\mathrm{d}^{m-1}\mathbf{v}}{\mathrm{d}t^{m-1}}\right) \qquad m = 2, 3, \ldots, M-1. \tag{28}$$

2. The second contribution is the trajectory from the midpoint $\mathbf{r}_{*/2}^{n+1/2}$ to the Eulerian arrival point $\mathbf{r}^{n+1}$. A Taylor series expansion about the arrival point involves only extrapolated velocities $\widetilde{\mathbf{v}}^{n+1}$, where the operator $\widetilde{(\cdot)}^{n+1}$ is defined by

$$\widetilde{(\cdot)}^{n+1} = 2\,(\cdot)^n - (\cdot)^{n-1}. \tag{29}$$

Table 1. Statistics for the slotted cylinder problem after one full rotation. The rows show: scheme (SL or LMCSL), resolution (i.e. number of grid points in each horizontal direction), and the different statistics listed in (17)–(22). The integration area is $\Omega = [0, 10]^2$ s^{-1} and the remaining model parameters are $\omega = 0.3635 \times 10^{-4}$, number of time steps (one rotation) = 96, $\Delta t = 1800.556$ s, $\psi_0 = 1.$, $\gamma = 25$, $\sigma = 15$, $s_w = 6$, $s_l = 25$

Scheme	res	rms	l_1	l_2	l_∞	$h_{\max}$	$h_{\min}$
Bicubic SL	51	0.0726	0.4189	0.3314	0.5768	0.84E-01	−.50E-01
Bicubic SL	101	0.0496	0.2264	0.2178	0.5813	0.11E+00	−.15E+00
Bicubic SL	151	0.0417	0.1605	0.1807	0.6073	0.11E+00	−.95E-01
Bicubic SL	201	0.0359	0.1214	0.1549	0.5295	0.10E+00	−.99E-01
LMCSL	51	0.0697	0.3905	0.3182	0.5698	0.11E+00	−.48E-01
LMCSL	101	0.0451	0.2005	0.1983	0.5145	0.11E+00	−.11E+00
LMCSL	151	0.0385	0.1491	0.1672	0.5051	0.10E+00	−.11E+00
LMCSL	201	0.0331	0.1116	0.1426	0.4334	0.93E-01	−.84E-01

Table 2. As in Table 1, but after 6 full rotations (i.e. 576 time steps) and only for a resolution of 101 × 101 grid points

Scheme	res	rms	l_1	l_2	l_∞	$h_{\max}$	$h_{\min}$
Bicubic SL	101	0.0701	0.3651	0.3079	0.6674	0.12E+00	−.47E-01
LMCSL	101	0.0683	0.3613	0.3003	0.6276	0.13E+00	−.46E-01

Table 3. As Table 1 but for the cosine hill problem (1 rotation). Note that the spatial resolutions are different than in Table 1. The model parameters are here: $\Omega = [0, 32 \times 10^5]^2 m$, $\omega = 0.3635 \times 10^{-5}$ s^{-1}, number of time steps (one rotation) = 71, $\Delta t = 8849.56$ s, $\psi_0 = 100$, $\gamma = 8 \times 10^5 m$, $\sigma = 4 \times 10^5$ m

Scheme	res	rms	l_1	l_2	l_∞	$h_{\max}$	$h_{\min}$
Bicubic SL	33	2.6663	0.4928	0.3046	0.3253	−.33E+00	−.21E-01
Bicubic SL	65	0.3673	0.0673	0.0407	0.0262	−.26E-01	−.93E-02
Bicubic SL	97	0.1095	0.0185	0.0121	0.0090	−.43E-02	−.50E-02
Bicubic SL	129	0.0482	0.0071	0.0053	0.0045	−.17E-02	−.29E-02
LMCSL	33	2.6621	0.5080	0.3042	0.3244	−.32E+00	−.21E-01
LMCSL	65	0.3654	0.0671	0.0405	0.0261	−.26E-01	−.93E-02
LMCSL	97	0.1092	0.0184	0.0120	0.0089	−.46E-02	−.50E-02
LMCSL	129	0.0480	0.0071	0.0053	0.0045	−.19E-02	−.29E-02

Table 4. As Table 3 but for 2 full rotations, that is, 142 time steps and only for a spatial resolution of 33 × 33 grid points

Scheme	res	rms	l_1	l_2	l_∞	$h_{\max}$	$h_{\min}$
Bicubic SL	33	3.6823	0.7244	0.4207	0.4492	−.45E+00	−.22E-01
LMCSL	33	3.6754	0.7104	0.4199	0.4489	−.45E+00	−.22E-01

For the second trajectory contribution we then have

$$\mathbf{r}_{*/2}^{n+1/2} = \mathbf{r}^{n+1} - \mathbf{C}_2, \tag{30}$$

where

$$\mathbf{C}_2 = \frac{\Delta t}{2}\tilde{\mathbf{v}}^{n+1} - \sum_{m=1}^{M-1} \frac{1}{(m+1)!}\left(-\frac{\Delta t}{2}\right)^{m+1} \frac{\mathrm{d}^m}{\mathrm{d}t^m}\left(\tilde{\mathbf{v}}^{n+1}\right). \tag{31}$$

Combining (25) and (30) the departure point is given in terms of the sum of two contributions

$$\mathbf{r}_*^n = \mathbf{r}^{n+1} - (\mathbf{C}_1 + \mathbf{C}_2). \tag{32}$$

To increase accuracy $\mathbf{C}_1$ is iterated. As has been common procedure in many SL operational models we also here use bilinear interpolations and two iterations to calculate $\mathbf{C}_1$. Note that the second contribution to the trajectories, $\mathbf{C}_2$, is based entirely on

Table 5. As Table 3 but for the rotating cone problem (1 rotation)

Scheme	res	rms	l_1	l_2	l_∞	$h_{\max}$	$h_{\min}$
Bicubic SL	33	1.9257	0.3537	0.2228	0.2832	−.28E+00	−.19E-01
Bicubic SL	65	0.4514	0.0683	0.0509	0.1043	−.10E+00	−.99E-02
Bicubic SL	97	0.2343	0.0307	0.0262	0.0637	−.64E-01	−.73E-02
Bicubic SL	129	0.1517	0.0171	0.0169	0.0509	−.51E-01	−.56E-02
LMCSL	33	1.9617	0.3851	0.2270	0.2873	−.29E+00	−.19E-01
LMCSL	65	0.4568	0.0686	0.0515	0.1065	−.11E+00	−.98E-02
LMCSL	97	0.2367	0.0309	0.0265	0.0655	−.65E-01	−.67E-02
LMCSL	129	0.1522	0.0171	0.0170	0.0521	−.52E-01	−.52E-02

Table 6. As Table 5 but for 2 full rotations, that is, 142 time steps and only for a spatial resolution of 33 × 33 grid points

Scheme	res	rms	l_1	l_2	l_∞	$h_{\max}$	$h_{\min}$
Bicubic SL	33	2.8536	0.5440	0.3302	0.3953	−.40E+00	−.21E-01
LMCSL	33	2.8681	0.5336	0.3319	0.3982	−.40E+00	−.20E-01

Table 7. As Table 1 but for the cyclogenesis problem after 16 time steps. The model parameters here are: $\Omega = [0, 10]^2$ and $\Delta t = 0.3125$ s. See text for details

Scheme	res	rms	l_1	l_2	l_∞	$h_{\max}$	$h_{\min}$
Bicubic SL	33	0.1204	0.0388	0.1239	0.8800	0.43E-01	−.43E-01
Bicubic SL	65	0.0647	0.0193	0.0657	0.6771	0.62E-01	−.62E-01
Bicubic SL	97	0.0496	0.0130	0.0502	0.4076	0.83E-01	−.83E-01
Bicubic SL	129	0.0418	0.0101	0.0422	0.3669	0.73E-01	−.73E-01
LMCSL	33	0.1044	0.0333	0.1074	0.7613	0.72E-01	−.72E-01
LMCSL	65	0.0541	0.0168	0.0549	0.4413	0.14E+00	−.14E+00
LMCSL	97	0.0454	0.0127	0.0460	0.4511	0.15E+00	−.15E+00
LMCSL	129	0.0379	0.0100	0.0383	0.4788	0.14E+00	−.14E+00

grid point values of the velocity field and is not iterated. For all trajectory calculations, including those in the traditional SL version of the code, we include the acceleration ($M = 2$). This issue is discussed further in Section 4.3. We note, that exactly the same trajectory algorithm is used for the SL and the LMCSL versions of the model.

4.2. The SISL set of prognostic equations

As, for example, Bates et al. (1993) the Coriolis term is treated with a semi-implicit scheme, that is, the time discretization for the semi-implicit momentum equations are

$$u^{n+1} = \left\{ u + \frac{\Delta t}{2} f v - \frac{\Delta t}{2} \frac{\partial(\phi + \phi_s)}{\partial x} \right\}_*^n + \frac{\Delta t}{2} f v^{n+1} - \frac{\Delta t}{2} \frac{\partial(\phi^{n+1} + \phi_s)}{\partial x} \tag{33}$$

$$v^{n+1} = \left\{ v - \frac{\Delta t}{2} f u - \frac{\Delta t}{2} \frac{\partial(\phi + \phi_s)}{\partial y} \right\}_*^n - \frac{\Delta t}{2} f u^{n+1} - \frac{\Delta t}{2} \frac{\partial(\phi^{n+1} + \phi_s)}{\partial y}. \tag{34}$$

The semi-implicit mass field prognostic equation is

$$\phi_{\mathrm{SL}}^{n+1} = \phi_{\mathrm{SL-exp}}^{n+1} + \frac{\Delta t}{2}\left(L_\phi^{n+1} - \widetilde{L}_\phi^{n+1}\right), \tag{35}$$

where

$$\phi_{\mathrm{SL-exp}}^{n+1} = \left\{ \phi - \frac{\Delta t}{2} \phi \nabla \cdot \mathbf{v} + \Delta t F_\phi \right\}_*^n - \frac{\Delta t}{2} (\phi \widetilde{\nabla} \cdot \mathbf{v})^{n+1} \tag{36}$$

and where linear terms at time step $n + 1$ in (35) are of the form

$$L_\phi = -\phi_0 \nabla \cdot \mathbf{v}. \tag{37}$$

In (37) ϕ_0 is the reference geopotential thickness used for the linearization of the non-linear term in the mass field equation.

Noise and stability problems have motivated alternative formulations of the non-linear terms in the mass field equation. The stability of different such schemes has been discussed in Durran and Reinecke (2004). For the present shallow water model it was not found necessary to introduce formulations alternative to those presented in (35) and (36).

Noise problems associated with orographic forcing and long time steps can be largely alleviated by using a small off-centring of the time averaged terms (Rivest et al., 1994). In this study, we do not introduce any off-centring.

For completeness the temporal discretization for the passive tracer equation reads

$$\psi_{\mathrm{SL}}^{n+1} = \left\{ \psi - \frac{\Delta t}{2} \psi \nabla \cdot \mathbf{v} \right\}_*^n - \frac{\Delta t}{2} (\psi \widetilde{\nabla \cdot \mathbf{v}})^{n+1}. \tag{38}$$

The spatial discretization of the prognostic equations is performed on an Arakawa C-grid (Arakawa and Lamb, 1977). All spatial derivatives are calculated using centred differencing. It is noted that the use of centred differences defines the traditional way of discretizing divergence which is used in the SL model.

Taking the x and y centred derivatives of (33) and (34), respectively, adding, and inserting in (35) gives an implicit equation in ϕ. Details can be found in Appendix A. The implicit elliptic equation is solved with a simple 'home made' overrelaxation solver. The actual solver used here is relatively inefficient and is not included in the CPU-timings referred to in section 6. It is noted, though, that efficient solvers for this type of problems do exist (see e.g. Bates et al., 1993)

4.3. The SI-LMCSL set of prognostic equations

As with the CISL scheme (Lauritzen et al., 2006) it is not trivial to combine the LMCSL scheme with the semi-implicit scheme in order to permit long time steps. In Lauritzen et al. (2006) a rather complex predictor–corrector technique was used. Here we follow a slightly different and simpler approach.

As mentioned above only the mass-field equations in (24) are solved with the new LMCSL scheme while no changes are introduced to the formulation of the momentum equations. For the ϕ field it might be expected that one could use (35) directly as it is, with the explicit forecast (36) replaced by its LMCSL version, that is,

$$\phi_{\mathrm{LM-x}}^{n+1} = \phi_{\mathrm{LM-exp}}^{n+1} + \frac{\Delta t}{2} \left(L_\phi^{n+1} - \widetilde{L}_\phi^{n+1} \right) \tag{39}$$

with

$$\phi_{\mathrm{LM-exp}}^{n+1} = \{ \phi + \Delta t F_\phi \}_{**}^n \quad . \tag{40}$$

This is, however, not possible and quickly leads to unacceptably noisy solutions. To understand the problem we need to consider the term

$$-\frac{\Delta t}{2} \widetilde{L}_\phi^{n+1} \tag{41}$$

which in (35) was introduced to eliminate the linear part of the extrapolated divergence term, that is, the last term in (36), and, in (35), replace it with the implicit term

$$\frac{\Delta t}{2} L_\phi^{n+1}.$$

The problem obviously is that the term (41) is inconsistent with the divergence term implicitly introduced in (40) because (41) is estimated from a divergence based on centred differences, whereas, in (40), it is determined from a divergence of the form (11). To achieve consistency, we therefore, replace the last extrapolated term (41) in (39) by

$$\frac{\Delta t}{2} \phi_0 \widetilde{\mathcal{D}}_{\mathrm{LM}}^{n+1}, \tag{42}$$

where $\widetilde{\mathcal{D}}_{\mathrm{LM}}^{n+1}$ is analogue to $\mathcal{D}_{\mathrm{LM}}^{n+1/2}$ but based on extrapolated winds only. In practice $\widetilde{\mathcal{D}}_{\mathrm{LM}}^{n+1}$ is determined from the $\mathbf{C}_2$ half time step contribution to the trajectories (see eq. 31), that is, a new set of weights $\hat{\tilde{w}}$, which gives

$$\widetilde{\mathcal{D}}_k^{n+1}{}_{\mathrm{LM}} = \frac{2}{\Delta t} \left(1 - \sum_{l=1}^{K} \hat{\tilde{w}}_{k,l} \right), \tag{43}$$

where the factor '2' shows that the trajectory contribution is only over a half time step and where subscripts k and l have the same meaning as in Section 2. After introducing the new term we obtain the following SI-LMCSL prognostic equation:

$$\phi_{\mathrm{LM}}^{n+1} = \phi_{\mathrm{LM-exp}}^{n+1} + \frac{\Delta t}{2} \left(L_\phi^{n+1} + \phi_0 \widetilde{\mathcal{D}}_{\mathrm{LM}}^{n+1} \right). \tag{44}$$

As for the traditional SISL scheme the SI-LMCSL forecast can be expressed as an explicit forecast $\phi_{\mathrm{LM-exp}}^{n+1}$ plus a so-called semi-implicit correction term. Apart from the replacement of the extrapolated linear divergence term the SI-LMCSL equations are, therefore, the same as for the traditional SL method. This means that all the SISL software, including the elliptic solver, can be reused.

The new SI-LMCSL scheme produces stable and smooth solutions even for time steps that are longer than what is possible with the traditional scheme, that is, maximum Courant number of the order 5–10. However, this can only be achieved if accelerations are taken into account when calculating $\phi_0 \widetilde{\mathcal{D}}_{\mathrm{LM}}^{n+1}$, that is, M in (31) must be at least 2. This and other issues related to the choice of semi-implicit parameters is discussed further in Section 6.1

For completeness we note that the LMCSL prognostic equation for the passive tracer, ψ, is identical to (6). That is, numerically, the passive tracer is forecasted with exactly the same scheme as used for $\phi_{\mathrm{LM-exp}}$ apart from the driving force in the later.

5. Tests with the semi-implicit shallow water model

A number of tests have been carried out to investigate the performance of the SI-LMCSL scheme. Here we present results from a typical test experiment with flow over a sharp isolated topographic feature. A passive tracer with sharp spatial variations is being transported in the developing non-linear divergent flow. The fields for topography (ϕ_s) and initial fluid surface geopotential ($\phi + \phi_s$) expressed in geopotential meters are shown in Fig. 5. The figure also includes the test initial passive tracer field, ψ. Only the fields for the 'Northern' hemisphere are plotted since, as mentioned above, symmetry is imposed around the centre-line of the integration domain. The reference geopotential depth ϕ_0/g used for the semi-implicit scheme is 6000 m. The number of grid points is 128 × 128, giving a grid distance of approximately 156 × 156 km. The mass fields plotted are purely

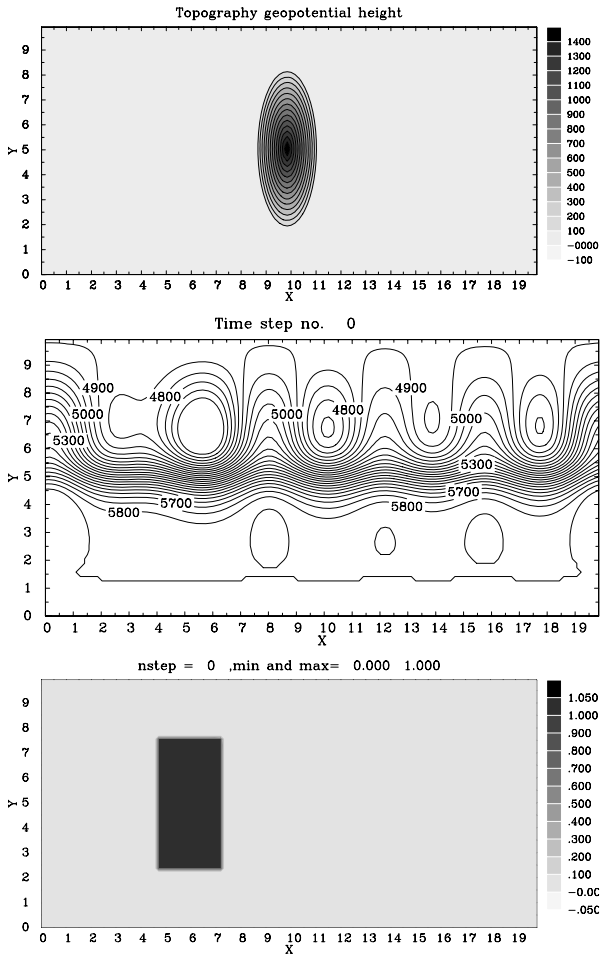

Fig. 5. Initial synthetic fields for the shallow water model test simulations. Only the upper half of the integration domain ('Northern hemisphere') is shown. From top: surface geopotential height ϕ_s/g in meters, fluid geopotential surface height $(\phi + \phi_s)/g$ in meters and the passive tracer concentration ψ per unit area.

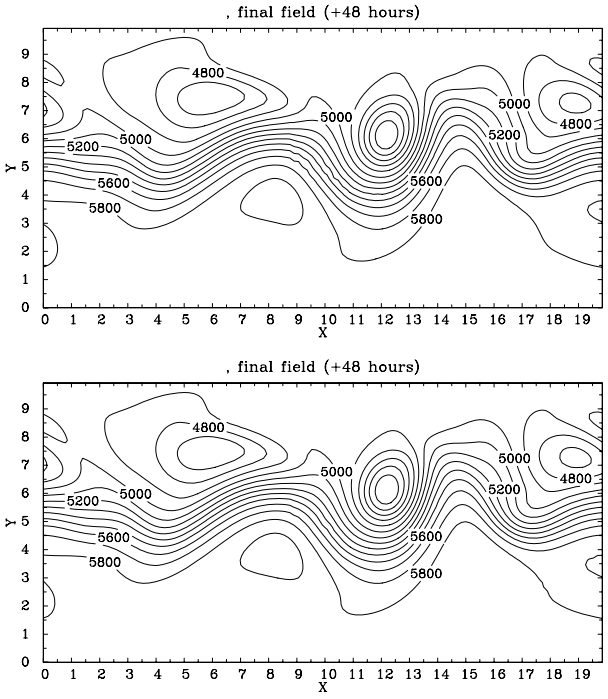

Fig. 6. Fluid geopotential surface height $(\phi + \phi_s)/g$ in meters after 48 hours of simulation in the upper half of the integration domain. Top: SISL. Bottom: SI-LMCSL. Both schemes are based on the same bicubic upstream interpolation scheme algorithm. See text for details about the simulations.

synthetic, while the wind fields are initialized simply to be in geostrophic balance with the initial $\phi + \phi_s$ field.

The numerical evolution of the $\phi + \phi_s$ field after 48 hours is shown in Fig. 6 for the classical SISL scheme based on bicubic interpolations and for the corresponding new SI-LMCSL scheme. The time step, Δt, used in these simulations is 3600 s. With the typical maximum simulated flow speeds of around 70 $\mathrm{m\,s^{-1}}$ this corresponds to a maximum diagonal (two-dimensional) Courant number

$$C = \sqrt{2}\frac{v_{\max}\Delta t}{\Delta x}$$

of approximately 2.3. It can be seen that although the semi-implicit scheme in the two models is rather different, the numerical solution is very similar. There is, however, a noticeable difference in the level of noise over and immediately downstream of the isolated mountain: in the SISL scheme this noise is clearly visible in the height field, while the level of noise is hardly discernible for the new SI-LMCSL scheme. This statement is not only true for the actual case presented here. The new scheme does not entirely prohibit mountain wave resonance (see e.g. Rivest et al., 1994; Lindberg and Alexeev, 2000), but a number of simulations at different spatial and temporal resolutions (not shown) indicate that the problem is significantly reduced as compared to SISL. Note that no off-centring was introduced in the

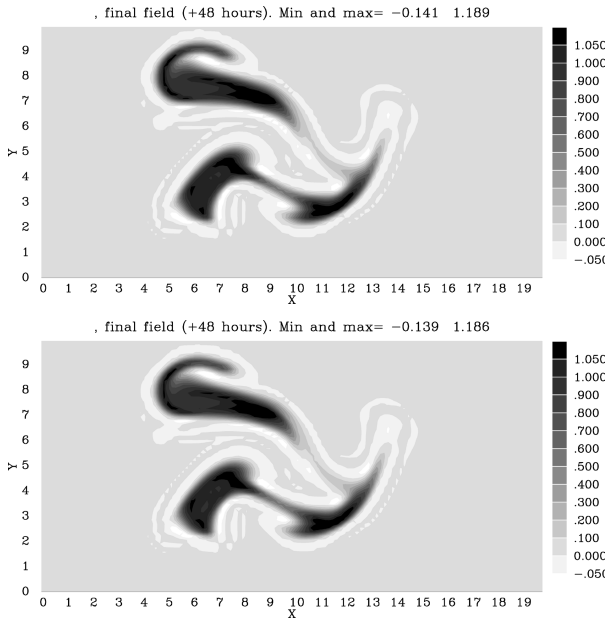

Fig. 7. As Fig. 6 but for the passive tracer concentration (ψ). The minimum and maximum simulated values are indicated on top of each panel.

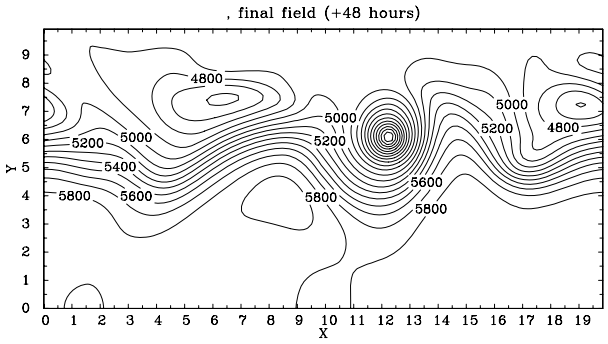

Fig. 8. As Fig. 6 (lower panel) but for the LMCSL scheme in a test setup where no accelerations were used in the calculation of $\mathbf{C}_2$ needed in the calculation of the semi-implicit correction term. The length of the time step was 1800 s as opposed to the 3600 s in the remaining shallow water model simulations.

semi-implicit scheme to alleviate the resonance problem (e.g. Rivest et al., 1994). The reasons for the apparent reduction in numerical mountain wave resonance in the SI-LMCSL model have not been understood yet but it must be related to the treatment of divergence and to the specific formulation of the semi-implicit scheme in LMCSL.

Numerically the new SI-LMCSL scheme is at least as stable as SISL, and typically allows time steps corresponding to a C value of 5–8 if the surface topography is not extreme (e.g. half of the fluid depth in only one row of grid points), in which case both schemes should not be run with C larger than about 2.5.

The numerical evolution of the passive tracer is shown in Fig. 7. As expected from all the above results the SL and LMCSL schemes are very similar indicating that the new scheme treats the quite strong divergence in the vicinity of the 'mountain' in a reasonable way. As for the passive tracer experiments the typical problems of non shape preservation is seen via the simulated artificial negative ψ values. The fact that some values are larger than one (the initial density) is, however, not a proof that the schemes are non shape preserving since the convergent flow, for example, around the uphill slope of the 'mountain' must lead to densities exceeding one.

6. Discussion

6.1. Semi-implicit parameters and model stability

The performance of the SI-LMCSL scheme depends strongly on the choice of M in (31). If an M value of 1 is chosen the solution becomes unrealistic with too deep lows and ultimately the model becomes unstable when the maximum Courant number exceeds about 2. Figure 8 shows an example of the resulting geopotential field after 48 h of simulation when $M = 1$ and with $\Delta t = 1800$ s, but with all other parameters unchanged relative to the standard setup used in Fig. 6. The unrealistic model behaviour is obvious and very different from any other model configurations—for example, a semi-implicit Eulerian spectral option—not reported or shown here. This is the motivation for including accelerations in all the trajectory calculations, that is, $M = 2$. For the traditional semi-implicit SISL scheme it is noted, though, that the model can run without inclusion of accelerations in the trajectory calculations and with forecasts (not shown) that are very similar to those presented in section 5

To understand the cause of the unrealistic behaviour associated with $M = 1$ in the SI-LMCSL scheme one may consider the terms L_ϕ^{n+1} and $\phi_0 \widetilde{\mathcal{D}}_{\mathrm{LM}}^{n+1}$ in (44) in the idealized analytical case of a stationary circular low with non-divergent balanced circulation (i.e. gradient wind balance). At any radius from the centre the term L_ϕ^{n+1} will be very close to zero because the centred difference approximation to divergence is small. If acceleration due to the flow curvature is not included the term $\phi_0 \widetilde{\mathcal{D}}_{\mathrm{LM}}^{n+1}$ will, however, tend to be negative in the vicinity of the low because, in this case, trajectory departure points estimated from Eulerian arrival point velocities will be located further away from the centre of the low than the Eulerian arrival points themselves. This means that we must have a net trajectory convergence up to a certain range of distances from the low (depending on the radial variation of the tangential flow speed) resulting in negative $\phi_0 \widetilde{\mathcal{D}}_{\mathrm{LM}}^{n+1}$ values. When the semi-implicit correction term in this example becomes negative the low will deepen artificially.

The model stability also depends on the ϕ_0 value used. It may be speculated that a ϕ_0 value which is well below the maximum geopotential depth could contribute to the problem seen when not including accelerations in the estimate of $\phi_0 \widetilde{\mathcal{D}}_{\mathrm{LM}}^{n+1}$. A number of tests have shown that this is not the case. Too small values of ϕ_0 do indeed lead to unrealistic and unstable solutions but the

nature of this problem is quite different and dominated by noise at smaller scales in deep fluid regions.

The estimate of $\phi_0 \widetilde{\mathcal{D}}_{\mathrm{LM}}^{n+1}$ needed in (44) introduces an addition numerical cost. Preventing this cost by usage of (39) instead of (44) does not seem possible even for very high values of ϕ_0 in combination with different choices of M in the trajectory calculations.

6.2. Generalizations

For any upstream type SL model it is simple to set up a corresponding LMCSL version with the same numerical accuracy simply by introducing the appropriate modification (7) of the interpolative weights. Although not being investigated here it is also possible to modify SL finite volume schemes such as the cell integrated SL method (e.g. Machenhauer and Olk, 1997; Nair and Machenhauer, 2002), CISL, along the same lines as those presented here for traditional grid point SL schemes. To achieve this one will need to estimate and modify the weights associated with an upstream spatial integration over a fixed regular domain corresponding to the extension of the Eulerian grid cells. The modification of the weights will approximate the effects of divergence/convergence, which in CISL is dealt with by integrating over smaller or larger upstream departure volumes. In this case the potential advantage of LMCSL would be that, computationally, integration over a fixed and regular spatial volume is much simpler than integration over a less regular volume of varying size.

There should in principle be no obstacles hindering constructing a LMCSL scheme based on a cascade interpolation approach such as in Nair et al. (1999). This can be achieved by introducing modifications of the weights associated with, for example, the cubic interpolations used in each of the spatial directions. Also in the cascade case it should be possible to simplify the finite volume schemes by Nair et al. (2002) and Zerroukat et al. (2002) and subsequent improved schemes. In this case one will need to introduce modifications of the weights determined by upstream one-dimensional integrations over fixed upstream distances (corresponding to the grid spacing) and thereby improve the numerical efficiency without loosing the accuracy. Test of a cascade LMCSL approach is an obvious subject for future work.

The LMCSL is very similar to the various recent finite volume SL schemes referred to here. Therefore, the generalization from two to three dimensions can be done along the lines used in other models. An obvious choice is to introduce a (semi-) Lagrangian vertical coordinate as in Lin (2004) and as in Lauritzen (2005). The similarity with other schemes also imply that generalization to spherical coordinates should be rather straightforward.

6.3. Numerical costs

Overall only relatively small code changes are needed to implement the new scheme into existing SL atmospheric models. All the experiments presented here have been performed on a single processor Intel Centrino CPU. The additional CPU (and wall clock) cost introduced by the LMCSL relative to the SL scheme is about 65% when only pure (divergent) transport is considered. This is the cost of the additional loop needed to calculate the modified weights in (7). The additional cost for adding a passive tracers is, however, slightly less than the same cost for the SL-scheme (=3–4% in case of bicubic interpolations) because no explicit treatment of the divergence term is needed. In the shallow water model where several other processes and equations are solved the relative overhead for the LMCSL over the SL is only about 15% in general. In this number the relative high cost of solving the elliptic equation in (A5) is not taken into account. Also in the shallow water model the additional cost of adding new tracers is slightly less in the LMCSL scheme than in the SL scheme.

6.4. Some remaining problems

One of the issues not studied in this paper is the desirable property of shape preservation, that is, monotonicity and positive definiteness. This will be dealt with in a subsequent paper where it will be shown that the LMCSL scheme can be combined with a new SL filter which not only ensures shape preservation, but also enhances the accuracy considerably, especially near sharp variations in gradients. The filter can easily be modified to ensure preservation of constancy in non-divergent flows as well.

Ongoing work regards a cure of the problem of mass-wind inconsistency (Jöckel et al., 2001) briefly introduced in Section 1. In the SI-LMCSL shallow water model presented here, one may believe that there is formal consistency between wind and tracer mass fields. This is, however, not the case due to the semi-implicit correction term which imposes changes to winds which are not considered in the trajectory calculations.

7. Summary

It has been demonstrated that a simple local correction of interpolative weights used in upstream SL type solutions to the continuity equation can ensure local mass conservation to machine accuracy in fluid dynamical models.

Indirectly the role of the weight corrections is to approximate the divergence term in the continuity equation for density which in traditional SL schemes is treated with a centred difference scheme.

In passive advection tests the weight corrections only introduce very small changes relative to a reference traditional non-conservative SL scheme based on bicubic interpolations.

The new LMCSL method to solve the continuity equation has been combined with the semi-implicit technique in a shallow water model to achieve a SI-LMCSL prognostic set of equations permitting long time steps and local mass conservation at the same time. To obtain reasonable results it was needed to include accelerations in the calculation of the trajectory departure points.

In plane geometry tests with a SI-LMCSL shallow water model including a varying bottom topography show results that are very similar to those obtained with a classical SISL reference model based on bicubic upstream interpolations. The SI-LMCSL scheme appears, however, to be less noisy than the SISL for high Courant numbers near sharp spatial topographic variations. Also for a passive tracer being transported by the shallow water model flow the LMCSL and the underlying SL scheme give very similar results.

8. Acknowledgments

The work was done as part of the CEEH center (www.ceeh.dk) sponsored by the Danish Council for Strategic Research, under the Danish Agency for Science, Technology and Innovation.

The new scheme was presented first time at the AGU-fall meeting in San Francisco 2006. This resulted in inspiring comments and suggestions for some of the verifications performed in this paper from the following persons: Bennert Machenhauer, David Williamson, Peter Hjort Lauritzen, Phil Rasch and Christiane Jablonovski. The author wish to express his gratitude to these persons.

The author is grateful for corrections to the manuscript by Ayoe Buus Hansen.

8. Appendix A: Semi-implicit semi-Lagrangian model formulation

This appendix describes the reference SISL model formulation.

The prognostic time difference—space differential equations for the shallow water equations are listed in (33)–(35). We now define the following explicit terms

$$
\begin{aligned}
U_E^{n+1} &\equiv \left\{ u + \frac{\Delta t}{2} f v - \frac{\Delta t}{2} \frac{\partial(\phi+\phi_s)}{\partial x} \right\}_*^n - \frac{\Delta t}{2} \frac{\partial(\phi_s)}{\partial x} \\
V_E^{n+1} &\equiv \left\{ v - \frac{\Delta t}{2} f u - \frac{\Delta t}{2} \frac{\partial(\phi+\phi_s)}{\partial y} \right\}_*^n - \frac{\Delta t}{2} \frac{\partial(\phi_s)}{\partial y} \\
\Phi_E^{n+1} &\equiv \left\{ \phi - \frac{\Delta t}{2} \phi \nabla \cdot \mathbf{v} + \Delta t F_\phi \right\}_*^n \\
&\quad - \frac{\Delta t}{2} \left(\phi \widetilde{\nabla \cdot} \mathbf{v} \right)^{n+1} \\
&\quad \left(= \phi_{\mathrm{SL-exp}}^{n+1} \quad \right).
\end{aligned} \tag{A1}
$$

The prognostic equations in (33)–(35) can then be written as

$$
\begin{aligned}
u^{n+1} &= U_E^{n+1} + \frac{\Delta t}{2} \left(f v - \frac{\partial \phi}{\partial x} \right)^{n+1} \\
v^{n+1} &= V_E^{n+1} + \frac{\Delta t}{2} \left(-f u - \frac{\partial \phi}{\partial y} \right)^{n+1} \\
\phi^{n+1} &= \Phi_E^{n+1} + \frac{\Delta t}{2} \phi_0 \left[(\widetilde{\nabla \cdot} \mathbf{v})^{n+1} - (\nabla \cdot \mathbf{v})^{n+1} \right].
\end{aligned} \tag{A2}
$$

After a little algebra we can now isolate u and v from the first two equations in (A2):

$$
\begin{aligned}
u^{n+1} &= \frac{1}{1+\left(\frac{\Delta t}{2} f\right)^2} \left[U_E^{n+1} + \frac{\Delta t}{2} \left(f V_E^{n+1} - \frac{\partial \phi^{n+1}}{\partial x} \right) \right. \\
&\qquad \left. - f \left(\Delta t/2\right)^2 \frac{\partial \phi^{n+1}}{\partial y} \right] \\
v^{n+1} &= \frac{1}{1+\left(\frac{\Delta t}{2} f\right)^2} \left[V_E^{n+1} + \frac{\Delta t}{2} \left(-f U_E^{n+1} - \frac{\partial \phi^{n+1}}{\partial y} \right) \right. \\
&\qquad \left. + f \left(\Delta t/2\right)^2 \frac{\partial \phi^{n+1}}{\partial x} \right],
\end{aligned} \tag{A3}
$$

whereby the divergence at time step $n+1$ can be expressed as

$$
\begin{aligned}
\nabla \cdot \mathbf{v}^{n+1} &= \frac{\partial u^{n+1}}{\partial x} + \frac{\partial v^{n+1}}{\partial y} \\
&= \frac{1}{1+\left(\frac{\Delta t}{2} f\right)^2} \frac{\partial}{\partial x} \left[U_E^{n+1} + \frac{\Delta t}{2} f V_E^{n+1} - \frac{\Delta t}{2} \frac{\partial \phi^{n+1}}{\partial x} \right] \\
&\quad + \frac{\partial}{\partial y} \left\{ \frac{1}{1+\left(\frac{\Delta t}{2} f\right)^2} \left[V_E^{n+1} - \frac{\Delta t}{2} f U_E^{n+1} \right. \right. \\
&\quad \left. \left. - \frac{\Delta t}{2} \frac{\partial \phi^{n+1}}{\partial y} + \left(\frac{\Delta t}{2}\right)^2 f \frac{\partial \phi^{n+1}}{\partial x} \right] \right\}.
\end{aligned} \tag{A4}
$$

Inserting (A4) into the last equation in (A2) we obtain the following elliptic equation

$$
\begin{aligned}
\phi^{n+1} &= \Phi_E^{n+1} + \frac{\Delta t}{2} \phi_0 \widetilde{\nabla \cdot} \mathbf{v})^{n+1} B(x,y) + C^{(1)}(y) \frac{\partial^2 \phi^{n+1}}{\partial x^2} \\
&\quad + \frac{\partial}{\partial y} \left[C^{(1)}(y) \frac{\partial \phi^{n+1}}{\partial y} \right] - \frac{\partial C^{(2)}(y)}{\partial y} \frac{\partial \phi^{n+1}}{\partial x},
\end{aligned} \tag{A5}
$$

where

$$
\begin{aligned}
B(x,y) &= A(y) \frac{\partial}{\partial x} \left(U_E^{n+1} + \frac{\Delta t}{2} f V_E^{n+1} \right) \\
&\quad + \frac{\partial}{\partial y} \left[A(y) V_E^{n+1} - A(y) \frac{\Delta t}{2} f U_E^{n+1} \right] \\
A(y) &= \frac{\frac{\Delta t}{2} \phi_0}{1+\left(\frac{\Delta t}{2} f\right)^2} \\
C^{(1)} &= \frac{\Delta t}{2} A(y) \\
C^{(2)} &= \left(\frac{\Delta t}{2}\right)^2 f A(y).
\end{aligned} \tag{A6}
$$

The elliptic eq. (A5) can be solved by efficient solvers. However, for simplicity we have here used a simple sequential over-relaxation, which is relatively slow. Note, that in the time-measurements of the performance of the schemes the time spent on the elliptic solver has been excluded. Once the elliptic equation has been solved the solution ϕ^{n+1} is used to calculate u^{n+1} and v^{n+1} using (33) and (34).

The variables are represented on an Arakawa C grid and for all spatial derivatives a centred second-order accurate scheme has been used. The finite difference representation of the terms

expressing divergence in (A5) has been formulated to ensure a vanishing global average. This is needed to obtain full mass conservation in case of the semi-implicit LMCSL scheme.

References

Arakawa, A. and Lamb, V. 1977. Computational design and the basic dynamical processes of the UCLA general circulation model. *Methods Comput. Phys.* **17**, 173–265.

Bates, J. R., Moorthi, S. and Higgins, R. W. 1993. A global multilevel atmospheric model using a vector semi-lagrangian finite-difference scheme. part I: adiabatic formulation. *Mon. Wea. Rev.* **121**, 244–263.

Cotter, C. J., Frank, J. and Reich, S. 2007. The remapped particle-mesh semi-lagrangian advection scheme. *Quart. J. Roy. Meteor. Soc.* **133**, 251–260.

Doswell, C. A. 1994. A kinematic analysis of frontogenesis associated with a nondivergent vortex. *J. Atmos. Sci.* **41**, 1242–1248.

Durran, D. R. and Reinecke, P. A. 2004. Instability in a class of explicit two-time-level semi-lagrangian schemes. *Quart. J. Roy. Meteor. Soc.* **130**, 365–369.

Hólm, E. 1995. A fully two-dimensional, nonoscillatory advection scheme for momentum and scalar transport equations. *Mon. Wea. Rev.* **123**, 536–552.

Jöckel, P., von Kuhlman, R., Lawrence, M. G., Steil, B., Brenninkmeijer, C. A. M., and co-authors. 2001. On a fundamental problem in implementing flux-form advection schemes for tracer transport in 3-dimensional general circulation and chemistry transport models. *Quart. J. Roy. Meteor. Soc.* **127**, 1035–1052.

Kaas, E., Guldberg, A. and Lopez, P. 1997. A lagrangian advection scheme using tracer points. In: *Numerical Methods in Atmospheric and Oceanic Modelling—The Andre J. Robert Memorial Volume* (eds C. Lin, R. Laprise and H. Ritchie), pp. 171–194. CMOS/NRC Research Press (Companion volume to Atmosphere-Ocean), Canada.

Laprise, L. P. R. and Plante, A. 1995. A class of semi-lagrangian integrated-mass (SLIM) numerical transport algorithm. *Mon. Wea. Rev.* **123**, 553–565.

Lauritzen, P. H. 2005. *An Inherently Mass-Conservative Semi-Implicit Semi-Lagrangian Model*. PhD Thesis, COGCI, University of Copenhagen, Niels Bohr Institute, Juliane Maries Vej 30, DK-2100 Copenhagen Denmark.

Lauritzen, P. H., Kaas, E. and Machenhauer, B. 2006. A mass-conservative semi-implicit, semi-lagrangian limited-area shallow water model on the sphere. *Mon. Wea. Rev.* **134**, 1196–1212.

Leonard, B. P., Lock, A. P. and Macvean, M. K. 1996. Conservative explicit unrestricted time step multidimensional constancy-preserving advection schemes. *Mon. Wea. Rev.* **124**, 2588–2606.

Leslie, M. L. and Purser, R. J. 1995. Three-dimensional mass-conserving semi-lagrangian scheme employing forward trajectories. *Mon. Wea. Rev.* **123**, 2551–2566.

Lin, S.-J. 2004. A "vertically lagrangian" finite-volume dynamical core for global models. *Mon. Wea. Rev.* **132**, 2293–2307.

Lin, S.-J. and Rood, R. B. 1996. Multidimensional flux-form semi-lagrangian transport schemes. *Mon. Wea. Rev.* **124**, 2064–2070.

Lindberg, K. and Alexeev, V. A. 2000. A study of the spurious orographic resonance in semi-implicit semi-lagrangian models. *Mon. Wea. Rev.* **128**, 1982–1989.

Machenhauer, B. and Olk, M. 1997. The implementation of the semi-implicit scheme in cell-integrated semi-lagrangian models. In: *Numerical Methods in Atmospheric and Oceanic Modelling—The Andre J. Robert Memorial Volume*, (eds C. Lin, R. Laprise and H. Ritchie), 103–126. CMOS/NRC Research Press (Companion volume to Atmosphere-Ocean), Canada.

McGregor, J. L. 1993. Economical determination of departure points for semi-lagrangian models. *Mon. Wea. Rev.* **121**, 221–230.

Nair, R. D., Coté, J. and Staniforth, A. 1999. Monotonic cascade interpolation for semi-lagrangian advection. *Quart. J. Roy. Meteor. Soc.* **125**, 197–212.

Nair, R. D. and Machenhauer, B. 2002. The mass-conservative cell-integrated semi-lagrangian advection scheme on the sphere. *Mon. Wea. Rev.* **130**, 649–667.

Nair, R. D., Scroggs, J. S. and Semazzi, F. H. M. 2002. Efficient conservative global transport schemes for climate and atmospheric chemistry models. *Mon. Wea. Rev.* **130**, 2059–2073.

Rančić, M. 1995. An efficient, conservative, monotone remapping for semi-lagrangian transport algorithms. *Mon. Wea. Rev.* **123**, 1213–1217.

Rasch, P. J. and Williamson, D. L. 1990. Computational aspects of moisture transport in global models of the atmosphere. *Quart. J. Roy. Meteor. Soc.* **116**, 1071–1090.

Reich, S. 2007. An explicit and conservative remapping strategy for semi-lagrangian advection. *Atm. Sci. Let.* **8**, 58–68.

Rivest, C., Staniforth, A. and Robert, A. 1994. Spurious resonant response of semi-lagrangian discretizations to orographic forcing: Diagnosis and solution. *Mon. Wea. Rev.* **122**, 366–376.

Robert, A. 1981. A stable numerical integration scheme for the primitive meteorological equations. *Atmos.-Ocean* **19**, 35–46.

Robert, A. 1982. A semi-lagrangian and semi-implicit numerical integration scheme for the primitive meteorological equations. *J. Meteor. Soc. Japan* **60**, 319–325.

Robert, A., Henderson, J. and Turnbull, C. 1972. An implicit time integration scheme for baroclinic models of the atmosphere. *Mon. Wea. Rev.* **100**, 329–335.

Staniforth, A. and Coté, J. 1991. Semi-lagrangian integration schemes for atmospheric models — a review. *Mon. Wea. Rev.* **119**, 2206–2223.

Temperton, C. and Staniforth, A. 1987. An efficient two-time-level semi-lagrangian semi-implicit integration scheme. *Quart. J. Roy. Meteor. Soc.* **113**, 1025–1039.

Xiao, F., Yabe, T., Peng, X. and Kobayashi, H. 2002. Conservative and oscillation-less atmospheric transport schemes based on rational functions. *J. Geophys. Res.* **107**(D22), 4609.

Zalezak, S. T. 1979. Fully multidimensional flux-corrected transport algorithms for fluid. *J. Comput. Phys.* **31**, 335–362.

Zerroukat, M., Wood, N. and Staniforth, A. 2002. SLICE: A semi-lagrangian inherently conserving and efficient scheme for transport problems. *Quart. J. Roy. Meteor. Soc.* **128**, 801–820.

Zerroukat, M., Wood, N. and Staniforth, A. 2005. A monotonic and positive definite filter for a semi-lagrangian inherently conserving and efficient (SLICE) scheme. *Quart. J. Roy. Meteor. Soc.* **131**, 2923–2936.

Zerroukat, M., Wood, N. and Staniforth, A. 2006. The parabolic spline method (PSM) for conservative transport problems. *Int. J. Numer. Meth. Fluid* **11**, 1297–1318.

Zerroukat, M., Wood, N. and Staniforth, A. 2007. Application of the parabolic spline method (PSM) to a multi-dimensional conservative semi-lagrangian transport scheme (SLICE). *J. Comput. Phys.* **225**(1) 935–948.